Journal of Machine Learning Research 23 (2022) 1-34 Submitted 10/20; Revised 4/21; Published 2/22

Scaling Laws from the Data Manifold Dimension

Utkarsh Sharma USHARMA7@JHU.EDU
Department of Physics and Astronomy
Johns Hopkins University
Baltimore, MD 21218, USA

Jared Kaplan JAREDK@JHU.EDU
Department of Physics and Astronomy
Johns Hopkins University
Baltimore, MD 21218, USA

Editor: Daniel Lee

Abstract

When data is plentiful, the test loss achieved by well-trained neural networks scales as a power-law $L \propto N^{-\alpha}$ in the number of network parameters N. This empirical scaling law holds for a wide variety of data modalities, and may persist over many orders of magnitude. The scaling law can be explained if neural models are effectively just performing regression on a data manifold of intrinsic dimension d. This simple theory predicts that the scaling exponents $\alpha \approx 4/d$ for cross-entropy and mean-squared error losses. We confirm the theory by independently measuring the intrinsic dimension and the scaling exponents in a teacher/student framework, where we can study a variety of d and α by dialing the properties of random teacher networks. We also test the theory with CNN image classifiers on several datasets and with GPT-type language models.

Keywords: scaling laws, data manifold, model capacity, under-parameterized, intrinsic dimension

1. Introduction

Neural Network based Machine Learning has made enormous progress in a wide variety of domains. Scale has been a key ingredient in this success: large amounts of computation, large datasets, and large models with millions or billions of parameters.

Not only is scale beneficial to performance, but the benefits from scale can be predicted precisely. Recent works Hestness et al. (2017, 2019); Rosenfeld et al. (2019); Kaplan et al. (2020) studying a variety of data modalities and model architectures all find the same scaling relation in the underfitting regime. In particular, the dependence of the test loss on the number of model parameters N has the following properties, and each suggests a corresponding question:

- As the number of model parameters N is increased, the cross-entropy test loss of well-trained and well-tuned models scales with N as a power-law

$$L(N) \propto \frac{1}{N^{\alpha}} \tag{1.1}$$

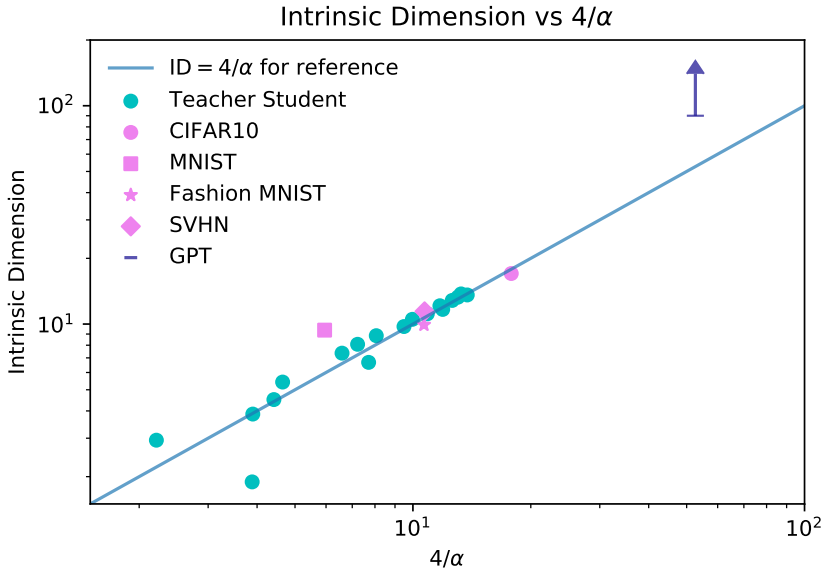

Figure 1: This figure shows the relationship between the measured intrinsic dimension (ID) of the data manifold and $\frac{4}{\alpha}$, where α is the model size scaling exponent. We include data from fully-connected teacher/student experiments, simple CNNs, and GPT-type Radford et al. (2018, 2019) language models (represented as a lower-bound due to large uncertainties with large IDs).

with observed values such as $\alpha \approx 0.076$ for language modeling Kaplan et al. (2020), and much larger $\alpha \approx 0.5$ observed for image classification Rosenfeld et al. (2019). Why do we encounter this simple functional form, and what determines the value of the exponent α?

- Scaling holds very accurately across a wide range of N, sometimes spanning many orders of magnitude Hestness et al. (2017, 2019); Kaplan et al. (2020). Why does scaling persist over a large range of model sizes, and what determines the $N_{\max}$ where it eventually breaks down?

- Empirically, the scaling exponent α may not depend greatly on model architecture. For example, LSTMs and Transformers scale similarly over a large range of N Kaplan et al. (2020), with losses differing only by an overall, N-independent factor. Why would scaling exponents be roughly independent of model architecture?

We will argue that a simple conjectural theory can address these questions while making a number of testable predictions.

1.1 Main Ideas and Organization of the Paper

The key idea is that neural models map the data to a manifold with intrinsic dimension d, and then use added capacity to carve up this manifold into ever smaller sub-regions. If

the underlying data varies continuously on the manifold, then the size of these sub-regions (rather than their number) determines the model's test loss. To shrink the size of the sub-regions by a factor of 2 requires increasing the parameter count by a factor of 2^d, and so the inverse of the scaling exponent $1/\alpha$ will be proportional to the intrinsic dimension d of the data manifold. We develop these ideas in detail in section 2.

The scaling exponent α can be measured by training a succession of models of varying size. To verify the theory on real-world datasets, we need an independent measurement of the intrinsic dimension. In subsection 2.3 of the same section, we measure the intrinsic dimension d within the final hidden layer[1] activations of trained networks, using the distances among nearest neighbor activation vectors Levina and Bickel (2005); Facco et al. (2017). We also explain why simpler methods like principal component analysis (PCA) don't suffice.

In section 3, we test the theory in a student/teacher framework, which makes it possible to scan over a large range of α and d and test more idiosyncratic features of the theory (see figure 2). We also perform tests using CNNs for image classification, and by measuring the intrinsic dimension of GPT-type models Radford et al. (2018, 2019), where scaling exponent have already been documented Kaplan et al. (2020).

We follow up with section 4 on related work and a discussion in section 5.

2. A Simple Theory for Scaling in the Underfitting Regime

In this section we explain our theory, beginning with a toy model to discuss properties of regression in section 2.1. Then in section 2.2 we argue[2] that the toy model can be applied to realistic neural networks with only a few small modifications. In section 2.3 we explain how we measure the dimension of the data manifold, a necessary step in validating the theory.

2.1 A Toy Model

Consider one of the simplest scenarios for multidimensional regression. We are given a Lipschitz function $f : [0,1]^d \to \mathbb{R}$, and we would like to approximate it as a piecewise constant function $c(x)$, by cutting $[0,1]^d$ into smaller hypercubes. If these hypercubes have a side length s, then we will have

$$N = s^{-d} \tag{2.1}$$

cubes, and so our approximation will depend on the N constant values $c(x)$ takes within each hypercube. If the loss is mean-squared error (MSE), then it will be bounded by

$$L = \int_0^1 d^d x |f(x) - c(x)|^2 \lesssim \lambda^2 \left(s^2 d\right) \tag{2.2}$$

where λ is the Lipschitz bound $|f(x+y) - f(x)| < \lambda |y|$, and we have ignored overall numerical factors. Translating the s-dependence into N, this means that $L(N) \lesssim \frac{1}{N^{2/d}}$ up to a constant factor.

1. It was shown in Ansuini et al. (2019) that the final hidden layer activations have the smallest intrinsic dimension in image classifiers. Our findings are largely consistent with this.
2. one might say conjecture; for a more sophisticated perspective in a simpler context see Bickel et al. (2007)

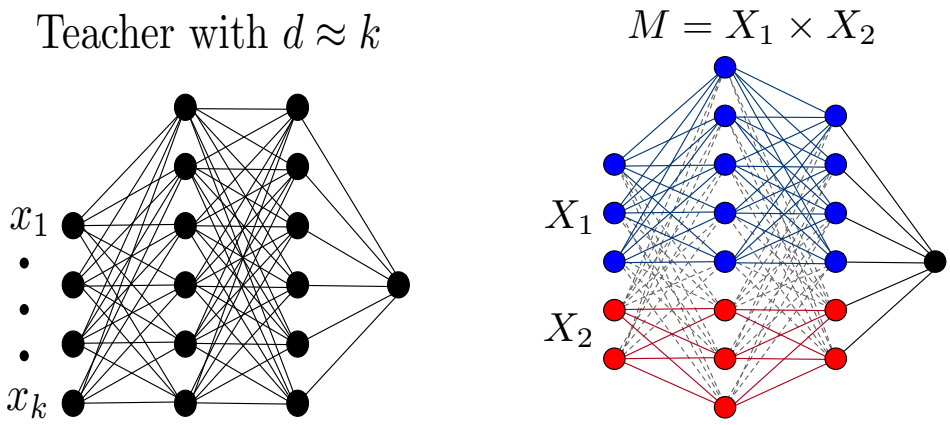

Figure 2: **Left**: This shows the setup of a teacher network, emphasizing how we can control the data manifold dimension via the number of input features k. **Right**: When the data manifold is a product and the teacher $T(X) = T_1(X_1) + T_2(X_2)$, then student networks can learn T by combining sub-networks and behaving, in effect, like an ensemble. Then we predict $4/\alpha \approx d_{\text{max}}$, the maximum d among the components.

If the model is piecewise linear instead of piecewise constant and $f(x)$ is smooth with bounded derivatives, then the deviation $|f(x) - c(x)| \propto s^2$, and so the L^2 loss will scale[3] as s^4. We would predict

$$L(N) \propto \frac{1}{N^{4/d}} \tag{2.4}$$

This will be important later, since networks with ReLU activations produce piecewise linear functions.

Finally, consider the case where $f_i(x)$ encode a smooth probability distribution over $i = 1, \cdots, k$ possibilities, and we replace the MSE loss with the KL divergence. If the $c_i(x)$ are a piecewise linear model for the logits, then we also find that $L \propto s^4$. So the KL and MSE losses will scale with the same exponent in N at a given value of d. We demonstrate this in appendix A.5; it is a simple consequence of the fact that the expansion of $D_{KL}(p||q)$ in $(q - p)$ begins at second order. Note that if we use a cross-entropy instead of the KL divergence, the loss will scale in the same way towards a fixed constant value, the entropy of the true distribution.

3. A straightforward generalization suggests that if $c(x)$ is composed of piece-wise k-degree polynomials, and we use a loss $|f - c|^p$, then

$$L(s) \propto s^{(k+1)p} \tag{2.3}$$

in the infinite data limit. But if p is large then $c(x)$ within each hypercube will utilize many parameters. We test the p-dependence of this prediction in figure 5.

2.2 A Conjectural Theory for Neural Networks

Neural Networks perform well on data with thousands or even millions of dimensions. It is widely believed that this is possible because neural networks map the data into a much lower-dimensional 'data manifold', preserving and focusing on the features that are relevant for the task.

We emphasize that the data manifold is a feature of both the dataset and the task or loss function that has been optimized. Classifiers need only attend to features relevant for classification. Similarly, in the case of autoregressive models the data manifold would consist only of the features necessary to predict the next token in a sequence. So the data manifold for such a model (as we are defining it) may have many fewer dimensions than the space of full sequences, such as complete images or text samples. Properties of the data manifold may also depend on the model that is learning it, such as its architecture and activation functions.

We can explain the observed scaling relations for NNs by applying our toy theory while replacing the ambient dimension of the dataset with the intrinsic dimension of the data manifold. If we perform regression with a neural network with ReLU activations and a mean-squared error or KL divergence loss, the analysis of section 2.1 implies[4]

$$L(N) \propto \frac{1}{N^\alpha} \quad \text{with} \quad \alpha \approx \frac{4}{d} \tag{2.5}$$

In the case where the function $f(x)$ depends in a generic way on d independent variables, we will confirm this prediction empirically in section 3.1 (see figure 1). We also explore some special data manifolds and other loss functions in section 2.4.

This theory also largely explains why the scaling relation holds over such a large range of N. To double the resolution with which the model differentiates different points on the data manifold, we need 2^d times more parameters. It's reasonable to expect that model performance improves smoothly when we change the resolution by an order-one factor. But this seemingly natural assumption implies that if $d \gg 1$, we will see smooth scaling with N over many orders of magnitude. We would predict that the range in ΔN over which smooth scaling holds satisfies $\log(\Delta N) \propto d$. This also strongly suggests $\log N_{\max} \propto d$, where $N_{\max}$ is the largest network size exhibiting power-law scaling, as we do not expect $N_{\min}$, the beginning of the power-law region, to increase with d. We discuss some reasons why power-law scaling may cease in section 2.2.2.

Finally, the theory suggests an interpretation for the fact that different NN architectures tend to have similar scaling exponents when applied to the same dataset. It would appear that a given dataset and task are associated with a data manifold of fixed dimension, and improvements in architecture do not greatly alter its properties. Network architectures that can achieve smaller d on the same dataset can be scaled up to achieve larger gains, and so we would expect smaller d to correlate with better performance.

The interpretation of $4/\alpha$ as the dimension of the data manifold has a close connection with the notion of fractal dimensions. Typically fractal dimensions measure how the number

4. Depending on the network architecture and parameter values, the network could represent a piecewise linear function with $C \gg N$ piecewise components Montufar et al. (2014). However, these C components cannot be independently configured to optimize the loss. Since there are only N independent degrees of freedom available, we expect N, rather than C, to determine the effective capacity.

of components needed to approximate a fractal scales as the components shrink. But we can reinterpret this definition by asking how many components are needed to obtain a certain quality of approximation to the underlying fractal. When we use the loss itself to measure the quality of the approximation, then $4/\alpha$ is proportional to the corresponding fractal dimension.

Before moving on, let us discuss a few subtleties.

2.2.1 A Bound, Not an Equality

The classic analysis we reviewed through the toy model in section 2.1 provides an upper bound on the loss for function approximation (regression in the infinite data limit) using piecewise constant or piecewise linear approximators. This bound becomes an estimate when the function being approximated is a generic Lipschitz function in d-dimensions. However, if the function has a simple, non-generic structure then the loss may decrease much more quickly with increasing model size. So we should expect that

$$\alpha \gtrsim \frac{4}{d} \tag{2.6}$$

In special cases where the true underlying function or distribution is non-generically simple, we may find that this inequality is far from saturation.

As a concrete example, consider a data manifold $M = X_1 \times X_2 \times \cdots \times X_n$ with loss $L(x) = \sum_i L_i(x_i)$, as suggested on the right of figure 2. In this case a fully connected neural network may learn[5] this decomposition, computing each $L_i(X_i)$ using a separate path through the network, and only combining these paths in the last layer. This would result in a scaling exponent determined by the maximum of the dimensions d_i of the manifolds X_i. We test $L(N)$ for product data manifolds in section 2.4.1 and verify these predictions.

We may end up finding $d > \frac{4}{\alpha}$ for other reasons. We will attempt to measure d among neural activations, but there may not be any single layer where the model compresses all of the data onto the data manifold. For example, one might imagine a scenario where different components of the manifold are processed or compressed in different layers of the network. And networks with non-ReLU activations (eg Transformers and ResNets) may mix and superimpose different data manifolds upon each other, obscuring the manifold structure and causing the measured dimension to exceed the true dimension.

2.2.2 Why Does Power-Law Scaling Break Down?

If the dataset size is finite, then power-law scaling with model size N will cease when we begin to overfit the data. Overfitting dominates performance on many real-world datasets, obscuring potentially clean scalings with N. We encounter it with CIFAR10 in figure 6 and on other datasets in appendix A.4.

Even in the infinite data limit, if the data contains any entropy or noise then the power-law scaling must eventually end with the loss reaching a final plateau. Scaling could also end for other, more interesting reasons. For example, perhaps beyond a certain point the loss can only improve by exploring a higher dimensional data manifold. This is possible if the

5. If the total loss does not decompose as a sum, it is less clear that the network can learn an effective decomposition, but it may still be possible.

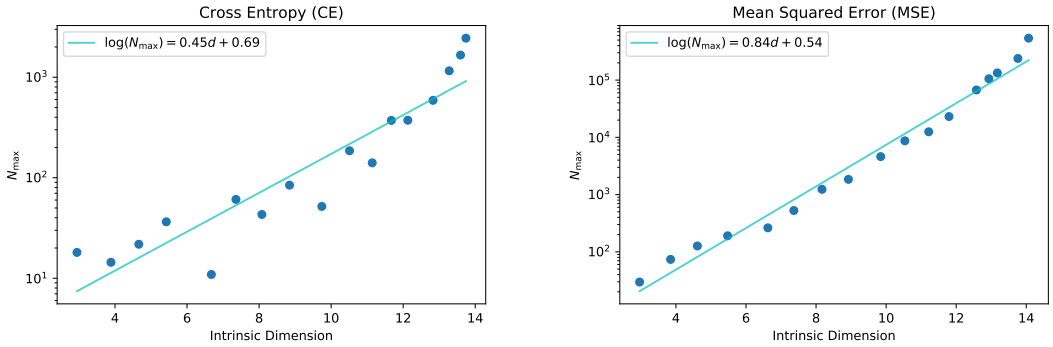

Figure 3: This figure estimates the behavior of N_{max}, the maximum network size where we find power-law scaling, as a function of the measured intrinsic dimension in student/teacher experiments. We determine N_{max} as the model size where the test loss reaches an arbitrarily chosen small value of 0.006, as a stand-in for the entropy of real data. We discuss this procedure in section 3.1.

data manifold has a pancake-like structure, with a small width that can only be dissected by models with very large capacity. We will explore the simplest possibility, where the data has entropy, with mock teacher/student experiments; see figure 3 for the result.

2.3 Measuring the Intrinsic Dimension of the Data Manifold

In section 2.2 we extended the toy model in order to make a variety of predictions relating the scaling of the loss with model size to d, the intrinsic dimension (ID) of the data manifold. In some of our experiments, we will control d by constructing generic functions of d inputs and then measuring α. But the theory would be tautological for real-world data if we could not independently measure the data manifold's ID.

We will define d by measuring the ID of neural activations as the network processes data from the distribution on which it was trained. There is an extensive literature on intrinsic dimension estimation (for a review see Camastra and Staiano (2016)). In most cases we use the simple two-nearest neighbors (TwoNN) method Facco et al. (2017), though we also compare to the MLE estimation Levina and Bickel (2005) method on which TwoNN was based.

To summarize the method, let r_k be the distance from a given datapoint to its kth nearest neighbor, and define $\mu_k \equiv r_k/r_1$. Then the cumulative distribution $C(\mu_k)$ takes the form

$$C(\mu_k) = \left(1 - \frac{1}{\mu_k^d}\right)^{k-1} \tag{2.7}$$

and so we can measure the intrinsic dimension d by using the relation

$$d = \frac{\log\left(1 - C(\mu_k)^{\frac{1}{k-1}}\right)}{\log \mu_k} \tag{2.8}$$

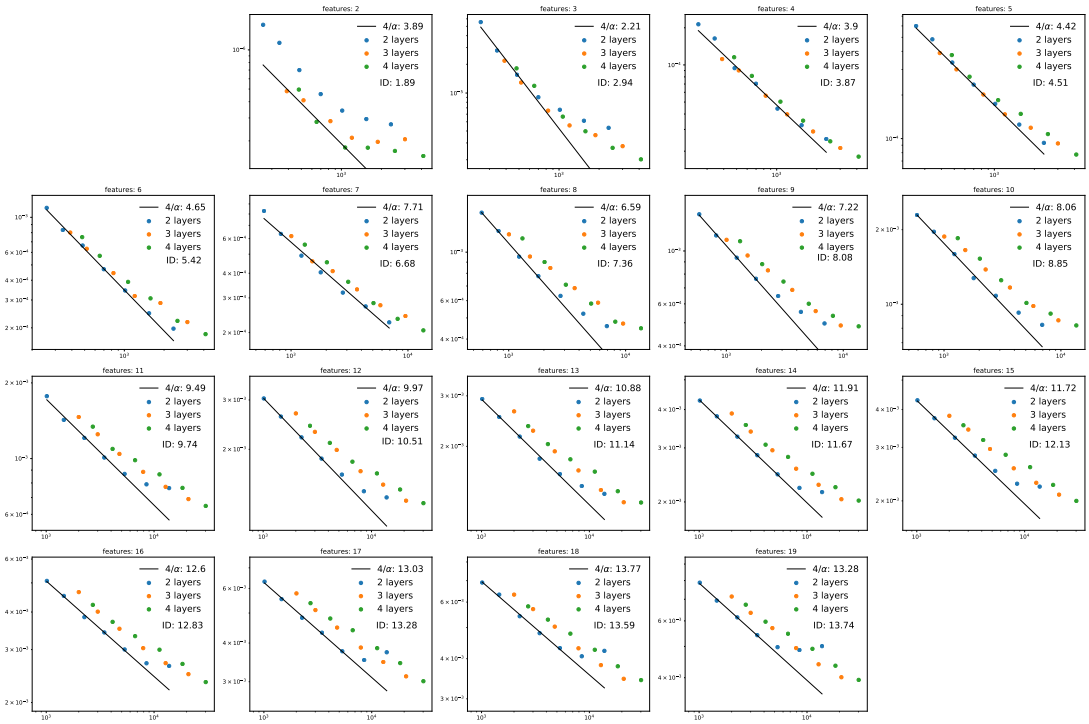

Figure 4: This figure shows $L(N)$ along with power-law fits for teacher/student experiments. The students learn from a randomly initialized 2-layer teacher with 2-19 features and use a cross-entropy loss. The students have 2,3, or 4 layers, but for $k > 5$ input features the 2-layer students perform best and determine the model-size scaling. The measured $4/\alpha$ increases linearly with the number of features, as shown in figure 7.

Practically speaking, we evaluate μ_k for every point on the manifold, and then apply linear regression to measure the slope d. We measure d using various k and verify that different values of k give consistent results. We also verify that the MLE method Levina and Bickel (2005) agrees with the TwoNN method. Fortunately, nearest neighbors can be efficiently identified Buitinck et al. (2013).

The TwoNN method (the case $k = 2$) has already been applied to neural networks Ansuini et al. (2019). There it was found that the dimension is smallest when measured using the activations of the final hidden layer of the network (immediately before the logits or output, so sometimes we refer to this as 'prefinal'). We will use these activations to measure d and compare to $1/\alpha$. For GPT-type models (and for some others as a test in appendix C) we show ID measurements for every layer.

For convenience we provide a self-contained derivation of these ID measurement algorithms and a minor extension ($k > 2$) in appendix B. We also provide several tests of the method in appendix C, using both synthetic and neural activation data. We find that the method is fairly accurate for $d \lesssim 20$, while for larger dimensions it's less reliable, and typically (but not always) underestimates the true dimension. Statistical errors from these methods are often fairly small (particularly from TwoNN), but we expect there may be larger systematic errors, as discussed in the appendices.

2.3.1 Why PCA and other linear methods don't suffice

Linear methods like principal component analysis (PCA) don't measure the intrinsic dimension of a manifold. For example, if data is distributed uniformly on the surface of a sphere S^2 in three dimensional space $\mathbb{R}^3$, then the intrinsic dimension of the data is 2. But PCA on this data would yield three equal components. Thus, PCA overestimates the dimension of a manifold that has a non trivial curvature.

2.4 Product Data Manifolds and Other Loss Functions

2.4.1 Product Data Manifolds $M = X_1 \times \cdots \times X_n$

If the data manifold takes the form $M = X_1 \times X_2 \times \cdots \times X_n$, with the underlying function of $x \in M$ decomposing as $F(x) = \sum_i f_i(x_i)$, then we expect that a neural network should be capable of separately modeling each f_i within separate blocks of activations, and then combining them in the final layer to compute the full F. This means that although the ID of M will be measured as $d_M = \sum_i d_{X_i}$, we should expect

$$\alpha \;=\; \frac{4}{\max(d_{X_i})} \tag{2.9}$$

as we discussed briefly in section 2.2.1, and demonstrate diagrammatically on the right of figure 2.

To test this prediction we use a vetted teacher network with 3 real inputs $T_3(x_1, x_2, x_3)$ and another vetted teacher taking 6 real inputs $T_6(x_1, \cdots x_6)$. Individually, these had ID $d_3 = 2.98$ and $d_6 = 5.31$ and their $L(N)$ exponents satisfied $\frac{4}{\alpha_3} = 3.3$ and $\frac{4}{\alpha_6} = 4.9$. These teachers each produce a pair of logits. We then constructed the new teacher functions with logits

$$T_{3+3}(x) \;=\; T_3(x_1, x_2, x_3) + T_3(x_4, x_5, x_6)$$

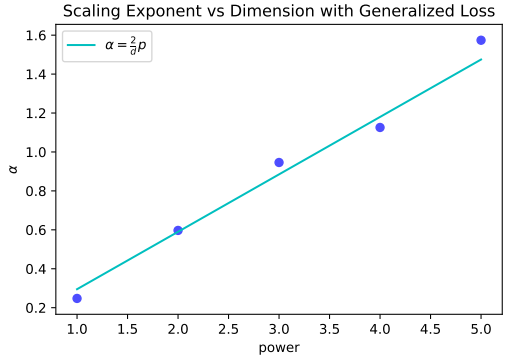

Figure 5: This figure shows the relationship between α and the power p when we use the generalized loss $|y - y^*|^p$. As expected from section 2.1, we find $\alpha = \frac{2}{d}p$. This is a student/teacher experiment with $d \approx 7$.

$$\begin{aligned} T_{3+3+3}(x) &= T_3(x_1, x_2, x_3) + T_3(x_4, x_5, x_6) + T_3(x_7, x_8, x_9) \\ T_{3+6}(x) &= T_3(x_1, x_2, x_3) + T_6(x_4, x_5, \cdots, x_9) \end{aligned} \tag{2.10}$$

and trained students to imitate these teachers using the cross-entropy loss. We then measured the resulting ID and α for these three product-manifold teachers. For the T_{3+3} and T_{3+3+3} cases we used two or three different teachers to make sure the network could not take advantage of the exact repetition of a single teacher.

As shown in figure 11, the results confirm our predictions. This provides a concrete example where we may find that $\alpha > \frac{4}{d}$ for reasons that the theory precisely anticipates. More importantly, it provides a very detailed test of our theoretical picture relating scaling exponents to properties of the data manifold.

2.4.2 Other Loss Functions

The factor of '4' in the relation $d \approx \frac{4}{\alpha}$ is derived from the behavior of the loss function and the expectation that networks with ReLU activations form piecewise linear functions. If we use a loss function such as $L(y, y^*) = |y - y^*|^p$ for regression, from the argument of section 2.1 we would expect

$$\alpha \approx \frac{2p}{d} \tag{2.11}$$

where the MSE case corresponds to $p = 2$. We verify this in figure 5 using a fixed teacher with intrinsic dimension $d \approx 7$, as measured in the usual student/teacher context.

3. Experiments and Results

In this section we discuss results from teacher/student experiments and various extensions, and also some tests using image classification and language modeling. We relegate a variety of technical details and a few minor observations to appendix A. We discuss potential errors in the ID measurement, along with several examples, in appendix C.

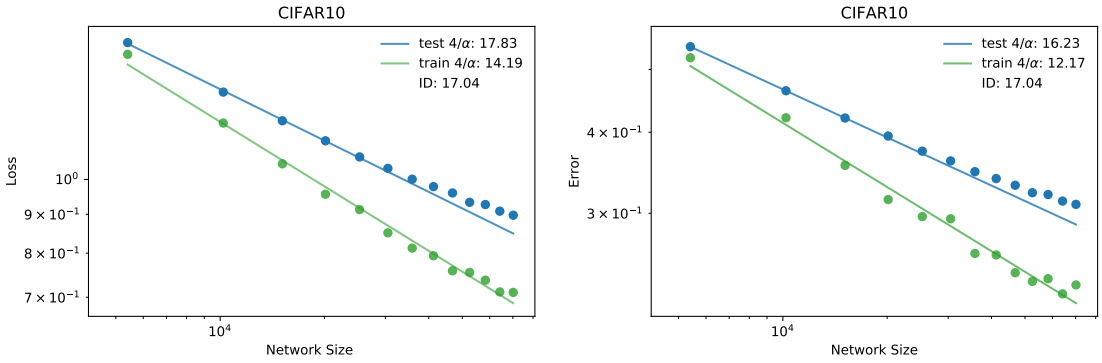

Figure 6: The left figure shows the test and training loss $L(N)$ for various sizes of CNN trained on CIFAR10, while the right figure shows error (1− accuracy). All results are evaluated at the early stopping step, where the test loss is minimized. We report test loss results in figure 1, but note that the exponents for accuracy are very close to those for loss.

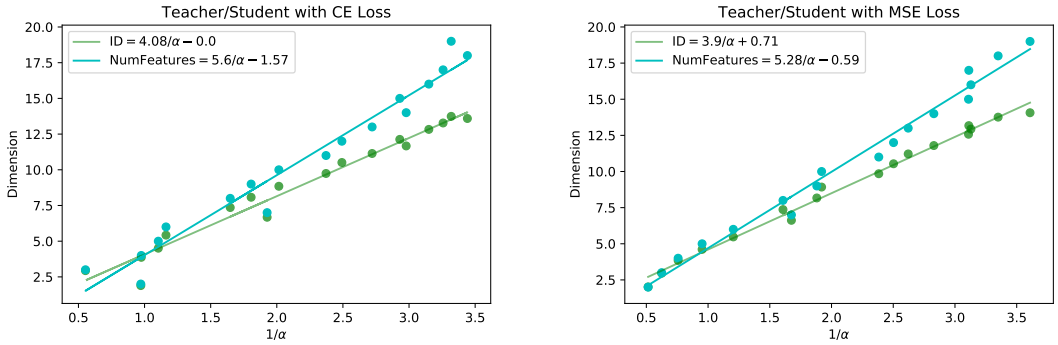

Figure 7: These figures show the correlation between the inverse scaling exponent $4/\alpha$ and both the measured intrinsic dimension and the number of input features (dimensions) in the teacher network. Both notions of dimension are linearly correlated with $1/\alpha$, and the intrinsic dimension scales almost exactly as $4/\alpha$, as predicted in section 2.2.

3.1 Teacher/Student with Random Teachers

We generate functions of $k = 2, 3, \cdots, 19$ input features using a randomly initialized, fully connected 'teacher' neural network with a 20-dimensional input space. To achieve $k < 20$ we simply zero out all other inputs to this single teacher. We refer to k as the number of features, and distinguish it from d, the intrinsic dimension, which we measure using the activations of trained student networks.

For each value of k, we train fully connected student networks of various widths and depths to imitate the outputs of the teacher. We work in the online setting, generating random inputs in $[-\frac{1}{2}, \frac{1}{2}]^k$ so the dataset size is effectively infinite.

We measure the intrinsic dimension from the activations of the final hidden layer of each trained student. We use $12,000$ activation vectors for each ID measurement. In all cases we find that using more nearest neighbors, as discussed in section 2.3, does not change the result significantly. The ID changes by only about 10% with the size of the student, as shown in figure 8. Details of the network topologies, training procedure, fits, errors, and ID measurements are documented in appendix A.2.

After training the students, we evaluate the loss $L_k(N)$ for each number of features k. Then we fit

$$L_k(N) = \frac{c}{N^\alpha} \tag{3.1}$$

to measure c, α for each k. The results of this process (with cross-entropy loss) are shown in figure 4.

3.2 Image Classification with Simple CNNs

Our goal with these experiments was to study a simple, all ReLU architecture that could scale down to a small enough size to avoid overfitting CIFAR10 Krizhevsky (2009). So we used a version of the default tutorial CNN in tensorflow Abadi et al. (2015), which we modified only by scaling the number of channels (ie the width). Figure 6 shows the scaling of the test loss with number of parameters N. Our only regularization was early stopping. The results match $4/\alpha = d$ quite well.

In an ideal test of the theory, we would measure α fully in the underfitting regime, with no distinction between train and test performance. But there is a train/test gap even for the smallest network sizes, so its unclear how to model the error in the α measurement. In addition to the test loss, we also measured the scaling of the training loss for these models, recording it at the early-stopping step, and found that it also scales similarly. Furthermore, note that on the right of figure 6 we record the error rate ($\equiv 1-$ accuracy), and find that it scales very similarly to the loss.

As with teacher/student experiements, we measure the intrinsic dimension from the activations of the final hidden layer of each trained student. We use $12,000$ activation vectors for each ID measurement. As before, we find that the ID changes by only about 10% across network sizes, as shown in figure 8.

We performed a very similar analysis on the MNIST LeCun and Cortes (2010), fashion MNIST Xiao et al. (2017), and SVHN Netzer et al. (2011) datasets using slightly smaller networks (see section A.4). We plot $L(N)$ in figure 15, which we have relegated to the appendix, as the power-law trends on these datasets are less clear than on CIFAR10.

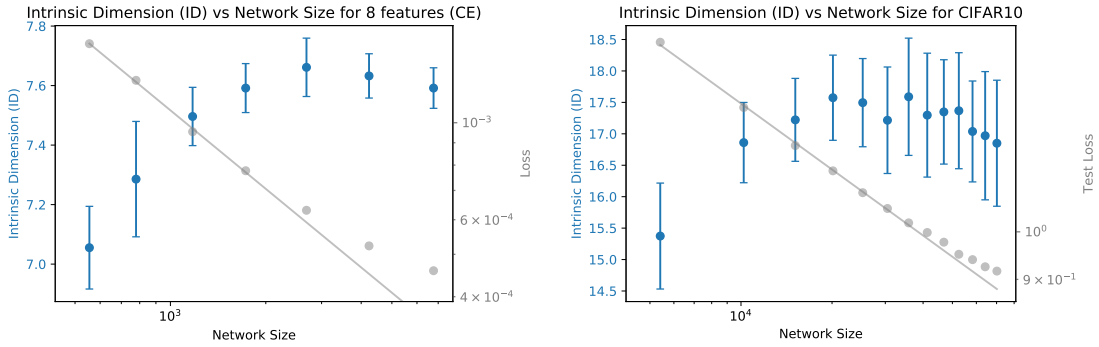

Figure 8: We show how ID measurements vary among different student network sizes N trained from the same teacher (left), and for CNNs on CIFAR10 (right). We display the test loss $L(N)$ for reference. The ID does not depend significantly on N, though it increases by about 10% among the various model sizes tested as N increases.

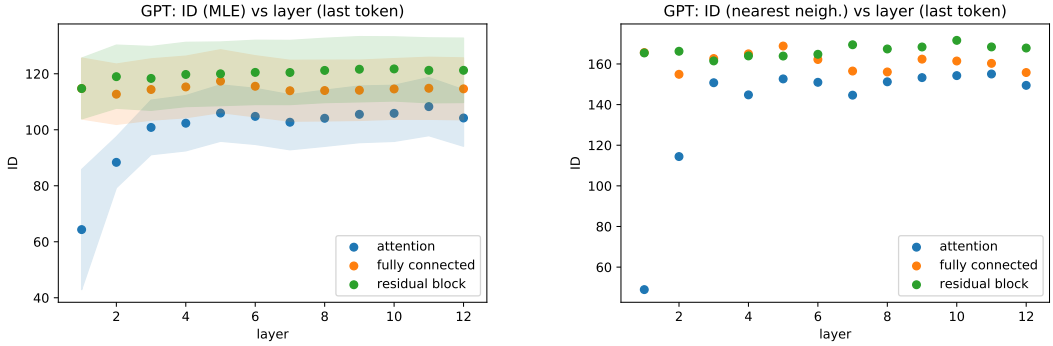

Figure 9: These figures show the ID estimates for the attention and fully-connected outputs of a 117M parameter GPT-type model, where $4/\alpha \approx 53$. The left figure shows results from the nearest neighbor method, with 2,3, and 4 neighbors, while the right plot shows results from the MLE method. The results roughly agree for the first layer, but the MLE method gives smaller IDs for later layers, and is likely an under-estimate.

Power-law exponents and IDs for CIFAR10 have been measured elsewhere using more powerful architectures, finding both a larger value of $\alpha \approx 0.5$ (for the error rate) Rosenfeld et al. (2019) and a smaller ID ≈ 8 Ansuini et al. (2019). We cannot make a clean comparison, but given that we find that the exponent for error-rate and loss scaling seem to be similar, these results appear to match our predictions.

3.3 Language Modeling with GPT-type Models

The GPT-type language models display power-law scaling of $L(N)$ over at least five orders of magnitude in N, with exponent $\alpha \approx 0.076$ Kaplan et al. (2020). This value of α is much smaller than those observed for many other datasets Rosenfeld et al. (2019), meaning that it allows us to probe a rather different regime, where we predict the quite large value $d \gtrsim 53$.

We generated activation vectors from the 'small' 117M parameter GPT-2 model using test data drawn from the same distribution as the training data Radford et al. (2018, 2019), and measured the IDs. Decoder-only Liu et al. (2018) Transformers Vaswani et al. (2017) have a residual structure with blocks including an attention mechanism and a fully-connected component. For each layer of blocks, one can measure the ID from the output of the attention mechanism, the fully-connected layer, or from the output of the residual re-combination.

The activations that contribute to the Transformer's outputs at any given token-position depend on all activations from earlier in the sequence, except for the case of the final layer (before multiplying by the unembedding matrix). Thus it is only the final hidden layer activations that can be said to capture the data manifold associated with the model's prediction for a single token. The mean loss over tokens has scaling exponent $\alpha \approx 0.076$, and from figure 21 of Kaplan et al. (2020) we see that α is roughly constant for tokens that occur late in any text sequence. So we use the activations from the last token in each sequence to measure the ID, though the ID does not vary significantly across token positions (see figure 10).

In figure 9 we plot the measured ID for the attention output, the fully connected output, and the combined output of the residual blocks for all layers. For these measurements we used 10,000 activation vectors, each from the last token in a different text sequence (for more details see appendix C.2). We see that unlike the case of image classifiers Ansuini et al. (2019), the ID is roughly constant across layers, with the exception of the first layer, where it is significantly smaller. If instead we measure the ID from the 1024 tokens in a single contiguous passage of text, we instead find an ID ≈ 7. This strongly suggests that the data manifold has a scale-dependent structure, and may not be well-characterized by a single intrinsic dimension.

It is tempting to observe that the intrinsic dimension of activations from the first attention layer is of order 50-80, which matches well with $4/\alpha$ for these models. One might argue that this bounds the total data manifold dimensionality entering the model through its input tokens. But as discussed above, this reasoning seems untrustworthy as an estimate of the data manifold dimensionality relevant for next-token predictions. So we take a conservative attitude and do not use early layer IDs as an estimate of the relevant ID for scaling.

We conclude that since $d > 90$, we have that $d \geq 4/\alpha \approx 53$, which accords with our expectations (see 2.2.1). Given the very small value of α in language modeling, it is satisfying to observe that the corresponding ID is very large. But it would have been more exciting to discover $\alpha \approx 4/d$ for language modeling. We do not know if the discepancy is due to added complexities from the structure of the Transformer, special structure on the data manifold itself, a scrambling of data manifolds due to the residual structure and attention mechanism, or some other oversimplification in our theory.

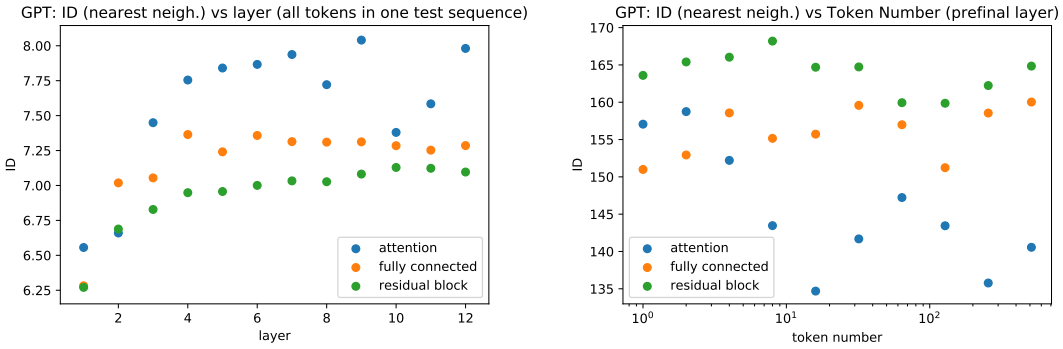

Figure 10: ID estimates from a single 1024-token text sequence (left) and the final layer ID as measured using tokens with fixed positions within distinct sequences (right). The data manifold associated with a single sequence has a much, much smaller dimension than the full manifold.

3.4 Summary of Predictions and Results

In this section we list the concrete predictions made by our theory, and their status based on our results[6] and information in the literature.

1. **Prediction:** Models with size $N \in [N_{min}, N_{max}]$ where the loss scales as a power-law in N all map the data to a manifold with the same intrinsic dimension d.

   Results: We measure the intrinsic dimension from the activations of the final hidden layer of each trained student. We use $12,000$ activation vectors for each ID measurement. In all cases we find that using more nearest neighbors, as discussed in section 2.3, does not change the result significantly. In figure 8 we show the measured ID of the final hidden layer of a student network with various sizes N, along with a plot of the loss $L(N)$. We see that the ID is approximately constant for these networks, though it does slowly grow by about 10% from the smallest to the largest student network and for CIFAR10 in figure 6. This prediction holds to about 10% for these models.

2. **Prediction:** In the range of N where the loss scales as $L(N) \propto \frac{1}{N^\alpha}$, we predict $\alpha \propto \frac{1}{d}$, where d is the intrinsic dimension of the data manifold for the dataset and task in question. If the network is composed of ReLU non-linearities and the loss is mean squared error or cross-entropy (or KL divergence), we predict

$$\alpha \gtrsim \frac{4}{d} \tag{3.2}$$

   with equality expected in the generic case.

   Results: We plot the relationship between $4/\alpha$ and either the number of features or the measured ID d for the teacher/student framework. The result, along with linear

6. Code for our experiments will be available at: `https://github.com/U-Sharma/NeuralScaleID`

fits, are shown in figure 7. For both the cross-entropy and MSE loss functions, $\frac{4}{\alpha} \approx d$. The inverse exponent $1/\alpha$ is linearly related to the number of input features k, but the multiplier is larger than 4. See figure 1 for the summary combining all datasets. Further, we show in figure 5 that this factor can be modified if we use other loss functions. For language modeling with GPT Radford et al. (2018, 2019), we know $\frac{4}{\alpha} \approx 53$ while we measure the intrinsic dimension as $d \geq 90$ (figure 9), in accord with the inequality, but quite far from equality.

3. **Prediction:** The maximum network size $N_{\max}$ where we obtain power-law scaling grows with d via $\log N_{\max} \propto d$. Larger d should correspond with much larger $N_{\max}$.

   Results: In section 2.2.2 we argued that scaling should end at an $N_{\max}$ that grows as $\log N_{\max} \propto d$. We would like to test this prediction with teacher/student experiments, but in this case the data has no entropy. So instead we will introduce an artificial threshold for the loss, as a fictitious stand-in for the entropy of real data. Then we simply ask at what $N_{\max}$ the loss $L(N)$ reaches this fixed, arbitrary value.

   We chose $L = 6 \times 10^{-3}$ as an arbitrary threshold in figure 3. Note that for the teacher networks with fewer features we used the power-law fit for $L(N)$ to estimate $N_{\max}$, as it was smaller than any network tested. This means we had to extrapolate $L(N)$, so these results are not purely empirical. We also compare $\log N_{\max}$ and d by defining $N_{\max}$ as the end of the purely empirical power-law scaling region for 2-layer students (due to a failure of optimization or numerical precision issues); these results are relegated to figure 12 in the appendix.

4. **Prediction:** If the data manifold $M = X_1 \times X_2 \cdots \times X_n$ and the loss $L(x) = \sum_i L_i(x_i)$, then we should replace the dimension of M with the maximum dimension of X_i when estimating α, as the network can behave as an ensemble, modeling each X_i independently (see the right of figure 2).

   Results: This was predicted in section 2.4.1. The results of the relevant experiments are in figure 11.

   While we verified all of the above predictions through experiments, we leave the next one to future work.

5. **Prediction:** The exponent α will not depend significantly on model architecture except through the intrinsic dimension d. Since larger α and smaller d lead to improved performance with scale, the best architectures will tend to have the smallest d.

   Results: In Ansuini et al. (2019) it was discovered empirically that better performing image classifiers have smaller d, and Kaplan et al. (2020) showed that LSTMs and Transformers have very similar exponents. We leave the measurement of both α and d across distinct architectures to future work.

The ID is typically a bit smaller than the number of input features. This may arise from a combination of two factors: the ID measurement may be underestimating the data manifold dimension, and randomly initialized networks may not provide sufficiently generic or non-linear functions of their inputs. We explore the second hypothesis in appendix A.3, where we show that by vetting the teacher networks we can improve agreement between ID

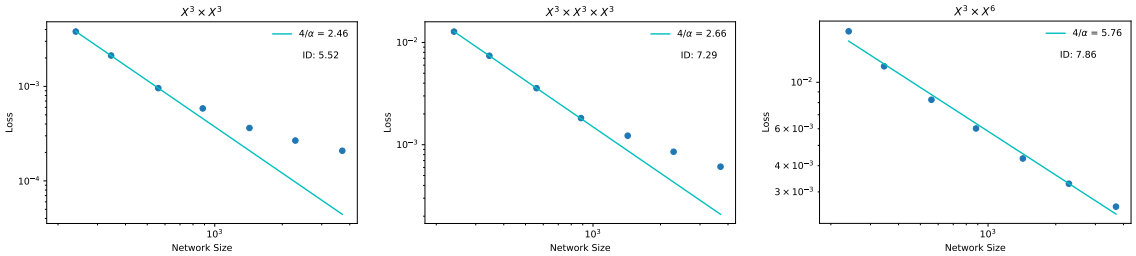

Figure 11: This figure shows results for α and d for product data manifolds with teachers T_{3+3} (left), T_{3+3+3} (middle), and T_{3+6} (right). We see that in all cases $\frac{4}{\alpha} \approx \max(d_i)$ among the product factor manifolds. The total measured IDs are approximately equal to the sum of the dimensions of the product factors, as expected.

and the number of input features. Figure 18 provides some idea of the potential errors in the ID measurements. Since the inputs themselves are drawn from a uniform distribution it is plausible that the ID is somewhat of an underestimate due to boundary effects.

4. Related Work

The theory of scaling we have advocated applies basic, 'textbook' Wasserman (2006) ideas from regression and density estimation. Our work was also partly inspired by similar scaling relations in random forest models; with some added assumptions, it is possible to prove them Biau (2012). As one passes from classical techniques, to random forests, and then to neural networks, the models become increasingly powerful but less and less amenable to a direct analysis. Nevertheless, we argue that similar principles apply and underly their scaling behavior. A similar overall perspective has been discussed by Bickel and collaborators Bickel et al. (2007).

There is a large literature on dimensionality estimation; for a nice overview see Camastra and Staiano (2016). We have primarily used the two nearest neighbor method Facco et al. (2017), which was based on the MLE method Levina and Bickel (2005) for distances among points in a local neighborhood. In neural image classifiers, the intrinsic dimension of the data manifold was studied Ansuini et al. (2019) using the TwoNN method. They demonstrated that the ID is much smaller than the dimension estimated via linear methods such as PCA, among other interesting results. Other authors have established a connection between ID and noisy labels Ma et al. (2018), and demonstrated that neural models can effectively identify a low-dimensional manifold in a larger ambient space Basri and Jacobs (2016). It would be interesting to understand the relationship between the data manifold and neural circuits Olah et al. (2020), and how the manifold changes when non-robust features are eliminated Ilyas et al. (2019). Recent work Spigler et al. (2019) relates data dimensionality and dataset size scaling exponents for kernel methods. The intrinsic dimension of the neural network parameter space has also been discussed Li et al. (2018).

Neural scaling laws have been studied in a number of papers. Perhaps the first work on the subject was Hestness et al. (2017). The more recent work Rosenfeld et al. (2019) studies scaling with model size and dataset size, both independently and simultaneously. Language models were studied in Kaplan et al. (2020), where scaling relations with model size, dataset size, training compute, and training steps were identified. EfficientNet Tan and Le (2019) displays near power-law scaling with model size, though these models are not in the underfitting regime.

5. Discussion

We have proposed a theory connecting the model-size scaling exponent with the intrinsic dimension of the data manifold. Many other neural scaling laws have been identified Hestness et al. (2017); Rosenfeld et al. (2019); Kaplan et al. (2020), including scalings with dataset size and compute budget, and fairly accurate power-law fits to learning curves. We have focused on scaling with model size in the infinite data limit because we expect it to be the simplest and most theoretically tractable scaling relation. Scaling with dataset size may involve issues of regularization, requiring a balance between bias and variance, while understanding the scaling with compute would require that we contend with optimization.

Nevertheless, neural scaling exponents with dataset size are often very similar[7] to model size exponents. One might argue that dataset size scaling can be understood as a consequence of interpolation between points on the data manifold, and so should have a similar relationship to the data manifold dimension. Recent works have made this case Spigler et al. (2019). Compute scaling exponents Kaplan et al. (2020) are also not far from model-size exponents, but combine optimization and model scaling. It seems most natural to interpret them by modeling learning curves, but perhaps optimization can be re-interpreted as the identification and dissection of the data manifold. Something like this will be necessary in order to explain the fact that larger models are much more sample efficient Kaplan et al. (2020) than small models. This may be the most impactful direction for future work.

It will be interesting to test this theory with a wider variety of models and datasets. Generative modeling may be the ideal setting, since the abundance of unlabeled text, image, and video data provides many opportunities to train large models on nearly unlimited datasets. In this context, it may be interesting to explore what the theory suggests for finetuning pre-trained generative models on downstream tasks. We would expect that these tasks benefit from the pre-established existence of the data manifold; perhaps finetuning can be understood as a process of zooming-in and refining performance in a small region of this manifold. It would also be interesting to understand how scaling relations for the loss compare to those for quantities that are not directly optimized, such as prediction accuracies. In the case of CIFAR10 we saw that accuracy and loss exhibit similar exponents. Finally, it's worth thinking about the extent to which larger models perform better in reinforcement learning Cobbe et al. (2019). Due to the non-stationary distribution in RL it may be difficult to understand model-size scaling quantitatively, and it's less clear how to apply our theory

7. Though in almost all cases Rosenfeld et al. (2019); Kaplan et al. (2020) dataset exponents are slightly larger. This runs somewhat counter to classical expectations Wasserman (2006), where the number of parameters determines a tradeoff between bias and variance, and dataset size exponents are smaller than the bias-scaling exponents that depend on model size.

in that context. A theory of sample efficiency scaling would be more likely to be relevant to RL.

Acknowledgments

We thank Yasaman Bahri, Ethan Dyer, Tom Henighan, Danny Hernandez, Jaehoon Lee, and Sam McCandlish for interesting discussions and feedback. We especially thank Ethan for sharing his notes on linear models and Yasaman for emphasizing that our theory of model size scaling might be re-purposed as a theory of dataset size scaling. JK has been supported in part by NSF grant PHY-1454083. This work was also supported in part by Open Philanthropy.

Appendix A. Technical Details and Minor Results

A.1 Fitting

To extract the scaling exponent α we need to fit power-laws to the empirical $L(N)$ for trained models with N parameters. For this purpose we simply fit straight lines to $\log L$ vs $\log N$, assuming that the error in $\log L$ was independent of N (ie we assumed Gaussian errors in $\log L$). We fit from the smallest value of N tested until the power-law behavior breaks down. This point is quite clear visually in most cases, as seen in figures 4, 13, and 6. For the case where we had networks with both different widths and different depths 4 we only used the networks that performed among the best at each model size (ie we used points on the 'convex hull' in the L vs N plane).

However, to avoid bias we determined the last point to include in the fit in the following way. We fit a circle (parameterized by its center and radius) to the first $n \geq 3$ points in the $\log L$ vs $\log N$ plane (starting at $N = N_{\min}$), and evaluated $r(n)$, the radius of the best-fit circle for each n. We then chose the value of n that achieved the maximal radius r, as this is the 'most linear' set of points. Finally, we fit a straight line $\log L = -\alpha \log N + b$ to this collection of points to determine α.

Note that this provides an alternative way to determine $N_{\max}$, the largest network in the power-law scaling region. This was the input for figure 12, where we show $N_{\max}$ as a function of d for teacher/student experiments.

The power-law scaling breaks down in CIFAR10 and other small image datasets due to overfitting. We do not have a complete understanding of why it breaks down for the teacher/student experiments, but it seems to be due to a failure of optimization, perhaps related to numerical precision. We note that the power-law behavior persists to larger model size and smaller loss with the deeper networks in figure 4.

A.2 Teacher/Student Experiments

A.2.1 Network Architectures

Our teacher networks had shape $[20, 600, 600, 2]$ (i.e. 20 dimensional input, two hidden layers of output dimension 600, and final layer ouput of dimension 2) for experiments with cross entropy loss (figures 4, 11 and 5), $[20, 600, 600, 1]$ for MSE loss (figure 13) and $[9, 240, 240, 2]$

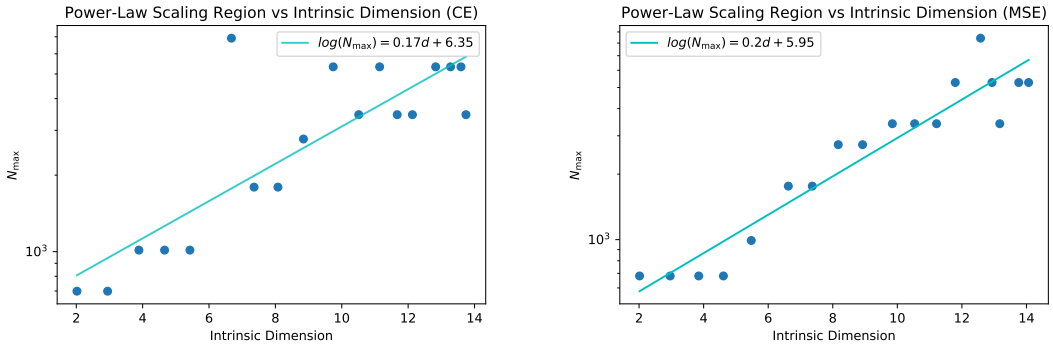

Figure 12: This figure shows the maximum number of parameters $N_{\max}$ at which we observe power-law scaling of $L(N)$, as a function of the intrinsic dimension, for teacher/student experiments. This $N_{\max}$ is determined as described in appendix A.1. The left plot uses cross-entropy loss, while the right uses MSE loss. This plot should be viewed as a more empirical (but less well understood) alternative to figure 3.

for cross entropy loss with vetted teacher (figure 14). The teachers are randomly initialized, with biases set to zero, and weights picked from a gaussian distribution of mean zero and standard deviation $1/\sqrt{N}$, where N is the input size of the layer. We experimented with including random non-zero biases, but did not find that they significantly alter the behavior of teachers.

For experiments with mean-squared error loss, the teacher and student networks each outputted a single real value. For experiments using a cross-entropy loss, networks output two logits, and we computed the cross entropy directly from these teacher outputs (ie we did not sample discrete values from the teacher, but used its exact output distribution). For cross-entropy experiments we used students with 2, 3, and 4 hidden layers, and let the best performing models define the $L(N)$ fits, while for MSE loss we simply used students with 2 hidden layers.

We ran 10 trials each for cross-entropy and MSE losses, and in each case selected the ones with the 9 lowest losses. Intrinsic dimension calculations were done using the same 9 networks. For vetted teacher experiments, we took 90 trials and computed the mean of the loss excluding the 10 worst performing students.

A.2.2 Optimization and LR Schedule

We use the ADAM optimizer Kingma and Ba (2014) with default settings except for the learning rate. In order to optimize effectively, we scanned over a grid of learning rates, and experimented with cosine, linear, and step-function learning rate schedules. We ended up using step function schedules for teacher/student experiments, and a constant learning rate for CIFAR10 and other image datasets, as these performed roughly as well or better than other choices. We did not find it necessary to vary the overall learning rate among different network sizes, but the schedules themselves were important for optimization. Our

Experiment (T/S)	student architecture	training steps	batch size	learning rate (ADAM)
(random) figures 7, 11, 5	MSE: [20,n,n,1] CE: [20,n,n,2]	0-200k 200-220k 220-240k	200 1000 4000	0.01 0.01 0.001
(vetted) figure 14	[9,n,n,2]	0-100k 100-150k 150-170k	200 200 200	0.01 0.001 0.0001

Table 1: Architectures and training schedules for Teacher/Student experiments in the paper, referenced by the figures in which the results are described.

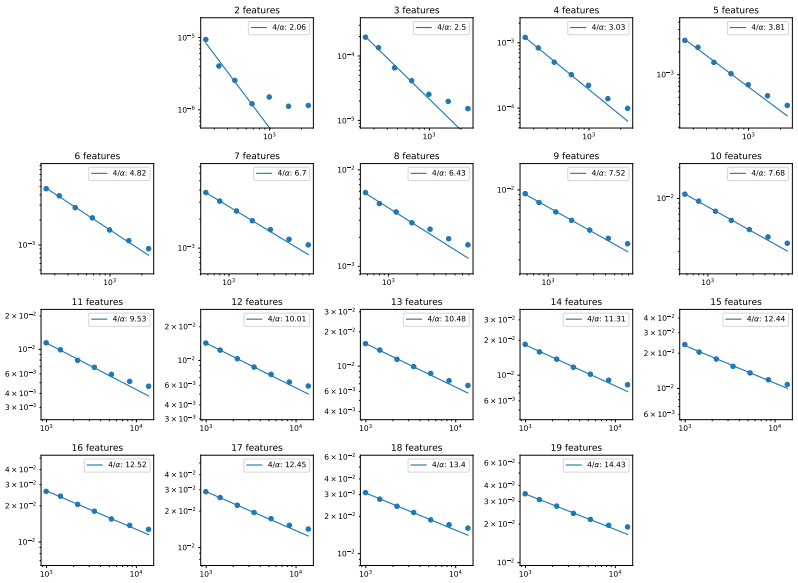

Figure 13: This figure shows $L(N)$ with a MSE loss for students (all with 2 hidden layers) learning from a randomly initialized teacher with 2-19 features. Figure 4 shows the results for cross-entropy loss.

learning rate schedules for the various teacher/student experiments in the paper (labeled by associated figures) are summarized in table 1.

A.3 Vetting Teachers to Increase Intrinsic Dimension

In figure 7, the ID is typically smaller than the number of features, especially when the latter is large. One might worry that this indicates ID measurements are inaccurate. In fact, we believe that this occurs partly because randomly initialized teacher networks do not typically produce fully generic functions of their inputs.

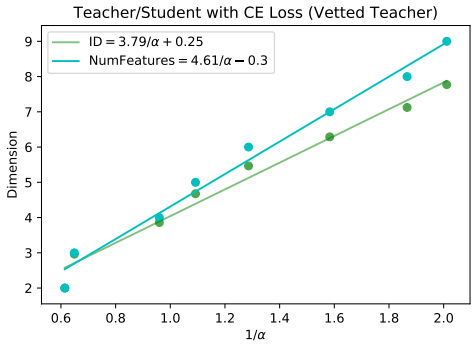

Figure 14: This figure shows the number of features and ID vs $1/\alpha$ for vetted teachers. ID is still smaller than the number of input features, but vetting partially closes the gap. Compare the slope of 4.61 for number of features vs $1/\alpha$ here to the left of figure 7, where the slope was 5.48. Slopes for ID vs $1/\alpha$ are very similar with or without vetting.

We can partially remedy this problem by generating a large number of teachers and vetting them, keeping only those that produce the most complicated and non-linear functions of their inputs. The result is pictured in figure 14, where we repeat the experiment of section 3.1 with up to 9 features. We see that sufficiently vetted teachers have ID nearly equal to their feature count, and that the relationship $\alpha \approx \frac{4}{d}$ continues to hold.

Presumably many vetting procedures could be successfully applied to filter the teacher networks. To increase the complexity and non-linearity of teachers so that ID would better match the number of input features, we followed this ad-hoc approach:

1. For a given teacher, we took a random slice along each input coordinate axis (i.e. the values of the other coordinates are chosen uniformly at random from $[-1/2, 1/2)$). We performed linear regression on this slice and computed the score(R^2, the coefficient of determination), and took the mean of the scores across coordinate axes. A low score implies more non-linearity.

2. We repeated this procedure 200 times and computed the mean score of all the trials. This is the score for the teacher.

3. We iterated over 5000 randomly generated teachers and selected the one with the minimum score.

A.4 CNNs on CIFAR10, MNIST, FMNIST, and SVHN

For CIFAR10 we used the architecture from the tensorflow CNN tutorial Abadi et al. (2015), and modified the channel width. The architecture is recorded in table 2.

The networks were trained for 50 epochs with the ADAM optimizer with default hyperparameters. We use 40 iterations of each network and average the loss (on log scale) over

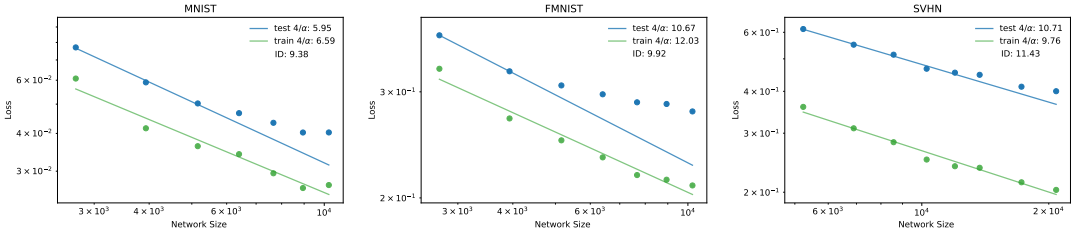

Figure 15: This shows train and test loss on MNIST, Fashion MNIST, and test loss on SVHN, along with the exponents and ID measurement.

Layer	Output shape
Conv2D	$(32, 32, n)$
MaxPooling2D	$(16, 16, n)$
Conv2D	$(16, 16, 2n)$
MaxPooling2D	$(8, 8, 2n)$
Conv2D	$(6, 6, 2n)$
Dense	(64)
Output	(10)

Table 2: Architecture of the CNN network used for CIFAR10. We chose n in the range $1 \leq n \leq 13$ to minimize overfitting. All convolutions were 3×3 with unit stride, and the images have 3 colors, so the network has a total of $N = 714 + 4640n + 54n^2$ parameters.

the iterations. Note that we record the test and training loss at the early stopping point where the test loss reaches its minimum value. These are the results in figure 6.

For MNIST LeCun and Cortes (2010), fashion MNIST Xiao et al. (2017), and SVHN Netzer et al. (2011), we use a slightly smaller network (3 instead of 4 hidden layers) with architecture shown in table 3. We used a smaller network in the hopes of identifying a power-law scaling region without significant overfitting.

For MNIST and fashion MNIST, we ran each network for 20 trials and took the mean loss (on log scale). The networks were trained for 50 epochs with the ADAM optimizer with default hyperparameters. As with CIFAR10, we take the minimum test loss during training (i.e. early stopping), and also report training loss at this point.

For SVHN, the networks were trained for 5 epochs with both training and additional datasets used for training (total 604k images), and test dataset (26k images) for testing. We used default hyperparameters.

A.5 Scaling of KL Divergence with Piecewise Linear Logits

We assume the logits $c_i(x)$ are linear in a small region of volume s^d we take to surround the origin, and that the underlying probability distribution $f_i(x)$ over k discrete choices is

Layer	Output shape
Conv2D	$(28, 28, n)$
MaxPooling2D	$(14, 14, n)$
Conv2D	$(12, 12, n)$
MaxPooling2D	$(6, 6, n)$
Dense	(32)
Output	(10)

Layer	Output shape
Conv2D	$(32, 32, n)$
MaxPooling2D	$(16, 16, n)$
Conv2D	$(14, 14, n)$
MaxPooling2D	$(7, 7, n)$
Dense	(32)
Output	(10)

Table 3: Architecture of the CNN network used for MNIST and fashion MNIST (left) and SVHN (right). All convolutions were 3×3 with unit stride.

smooth. The loss in this region is

$$L = \sum_{i=1}^{k} \int d^d x f_i(x) \log \frac{f_i(x)}{q_i(x)} \tag{A.1}$$

where $\log q_i(x) = c_i(x) + \log\left(\sum_{j=1}^{k} e^{c_j(x)}\right)$. If we write $q_i(x) = f_i(x) + \delta_i(x)$ then as is well known

$$\begin{aligned} L &= \sum_{i=1}^{k} \int d^d x f_i(x) \log \frac{f_i(x)}{f_i(x) + \delta_i(x)} \\ &= \int d^d x \sum_{i=1}^{k} f_i(x) \left(0 - \frac{\delta_i(x)}{f_i(x)} + \frac{1}{2}\left(\frac{\delta_i(x)}{f_i(x)}\right)^2 + \cdots\right) \\ &\approx \int d^d x \sum_{i=1}^{k} \frac{1}{2} \frac{\delta_i(x)^2}{f_i(x)} \end{aligned} \tag{A.2}$$

After optimization the linear $c_i(x)$ will determine a $\delta_i(x)$ that is quadratic in x, and so the loss per unit volume will scale as s^4, as claimed.

Appendix B. Review of Intrinsic Dimension Estimation Methods

In this section we review the two nearest neighbor method Ansuini et al. (2019) and explain that it can be extended to k-nearest neighbors. Then we note that the same analysis derives the maximum likelihood method Levina and Bickel (2005).

B.1 The Two Nearest Neighbor Method

Assume that points are drawn from a distribution with density $\rho(x)$ with support on a d-dimensional manifold in a potentially much higher dimensional ambient space. We will see that $\rho(x)$ drops out of our results, assuming that it is constant across the first few nearest neighbors, so we will drop its explicit x-dependence in what follows.

The probability of finding n points from the dataset in a region with d-dimensional volume V is Poisson:

$$P_n(V) = \frac{(\rho V)^n}{n!} e^{-\rho V} \tag{B.1}$$

To see this, note that in an infinitesimal volume δV, $P_0 = 1 - \rho\delta V$ and $P_1 = \rho\delta V$, with all $P_{n>1} = 0$. Thus the generating function for P_n in a finite volume V can be found by taking the product of binomial distributions over all δV in V, giving

$$G(x; V) = \lim_{\delta V \to 0} ((1 - \rho\delta V) + x\rho\delta V)^{\frac{V}{\delta V}} = \sum_{n=0}^{\infty} \frac{(x\rho V)^n}{n!} e^{-\rho V} \tag{B.2}$$

The coefficients of x^n are the P_n above.

With this result in hand, we can consider the distribution of nearest-neighbor distances. Consider some point in the dataset. The probability for its nearest neighbor to be in $[r_1, r_1 + dr]$ is given by the product of the probability that there are no points in $r < r_1$ times the probability of finding a point in the shell $r_1 < r < r_1 + dr$, which is

$$P(r_1)dr_1 = \left(d\rho\omega_d r_1^{d-1} dr_1\right) e^{-\rho\omega_d r_1^d} \tag{B.3}$$

where ω_d is the volume of a unit d-ball. This result easily generalizes to the case where there are many r_i corresponding to the first k nearest neighbors. For example for two nearest neighbors we find

$$P(r_1, r_2)dr_1 dr_2 = (\rho\omega_d d)^2 e^{-\rho\omega_d r_2^d} r_1^{d-1} r_2^{d-1} dr_1 dr_2 \tag{B.4}$$

since we are demanding that there are two points on two infinitesimal shells at radii r_1, r_2 and no points otherwise.

Now we can compute the distribution over nearest neighbor distances, and their ratios. The TwoNN method Ansuini et al. (2019) is based on the distribution of the ratio $\mu_2 = r_2/r_1$, which we can compute by integrating over r_1, r_2 while fixing their ratio:

$$\begin{aligned} P(\mu_2) &= \int dr_1 dr_2 \delta\left(\mu_2 - \frac{r_2}{r_1}\right) (\rho\omega_d d)^2 e^{-\rho\omega_d r_2^d} r_1^{d-1} r_2^{d-1} \\ &= \int dr_1 (\rho\omega_d d)^2 e^{-\rho\omega_d \mu^d r_1^d} r_1^{2d-1} \mu_2^{d-1} \\ &= \frac{d}{\mu_2^{d+1}} \end{aligned} \tag{B.5}$$

This means that the cumulative distribution for μ_2 is

$$C(\mu) = \int_1^{\mu} \frac{d}{\mu_2^{d+1}} d\mu = 1 - \frac{1}{\mu_2^d} \tag{B.6}$$

This means that *we can identify the dimension d by measuring the slope of a linear fit of* $\log \mu_2$ *vs* $\log(1 - C(\mu_2))$. That's the TwoNN method, as seen in figure 16.

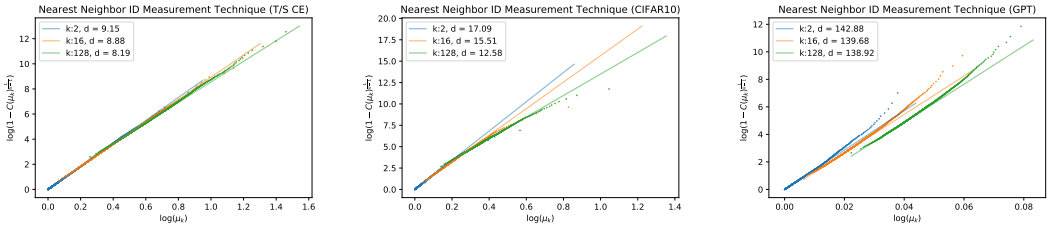

Figure 16: This figure shows the relationship in equation B.16, which we use to determine the ID using the nearest neighbor method. We display examples using teacher/student data, CIFAR10, and GPT.

B.2 Extension to k-Neighbors and MLE

The beauty of the TwoNN method Ansuini et al. (2019) is that it uses very short-distance information, and so it's plausible that the density $\rho(x)$ can be well-approximated as a constant. A down-side of this method is that it primarily measures the dimension on short scales. This can be mitigated by applying the method while sampling different numbers of points from the data distribution, but it's also easy to validate the TwoNN method by simply using more neighbors.

Let's see what happens with three neighbors, and then we will generalize. We can compute the distribution of $\mu_2 = r_2/r_1, \mu_3 = r_3/r_1$, and use it for validation. We have

$$\begin{aligned} P(\mu_2, \mu_3) &= \int dr_i \delta\left(\mu_2 - \frac{r_2}{r_1}\right) \delta\left(\mu_3 - \frac{r_3}{r_1}\right) (\rho\omega_d d)^3 e^{-\rho\omega_d r_3^d} (r_1 r_2 r_3)^{d-1} \\ &= \int dr_1 (\rho\omega_d d)^3 e^{-\rho\omega_d \mu_3 r_3^d} r_1^{3d-1} \mu_2^{d-1} \mu_3^{d-1} \\ &= \frac{2d^2 \mu_2^{d-1}}{\mu_3^{2d+1}} \end{aligned} \tag{B.7}$$

Intuitively, large μ_3 becomes unlikely because it implies that there are few points inside a large radius, but with fixed μ_3, a larger value of μ_2 is more probable due to the larger volume at large radius.

We find a nice simplification when we study $P(\mu_3)$ and its cumulative distribution after marginalizing over μ_2. The probability distribution is

$$P(\mu_3) = \int_1^{\mu_3} d\mu_2 \frac{2d^2 \mu_2^{d-1}}{\mu_3^{2d+1}} = \frac{2d}{\mu_3^{2d+1}} \left(\mu_3^d - 1\right) \tag{B.8}$$

The cumulative distribution is then

$$C(\mu_3) = \left(1 - \frac{1}{\mu_3^d}\right)^2 \tag{B.9}$$

Thus we also find a simple method for identifying d based on μ_3 alone, namely

$$d = \frac{\log\left(1 - \sqrt{C(\mu_3)}\right)}{\log \mu_3} \tag{B.10}$$

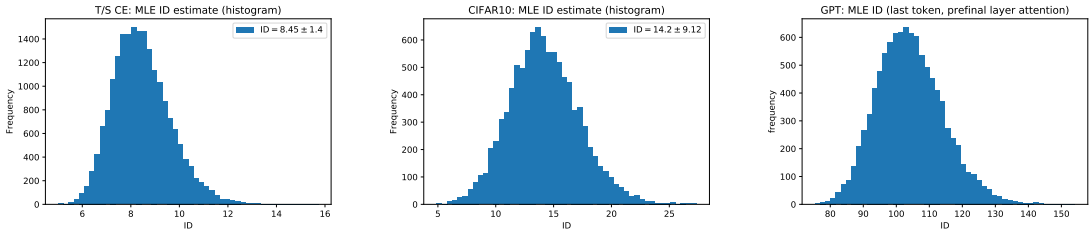

Figure 17: These figures show a histogram of the results for d from MLE (with 100 neighbors) among all of the points used for measurement. On the left we have a teacher with 10 features, in the middle we have the $n = 5$ CNN trained on CIFAR10, while on the right we have the GPT model's prefinal attention output for the last token in the text sequence. Smaller numbers of neighbors typically give larger IDs.

This directly generalizes the TwoNN; in practice we measure d via a linear fit to the numerator as a function of the denominator in this expression.

Generalizing to k neighbors, the probability distribution for $\mu_2, \cdots, \mu_k$ is

$$P(\mu_i) = d^{k-1}(k-1)! \frac{\prod_{i=2}^{k-1} \mu_i^{d-1}}{\mu_k^{1+d(k-1)}} \tag{B.11}$$

for $\mu_i = r_i/r_1$. This can be used directly for maximum likelihood estimation Levina and Bickel (2005). If we maximize $\log P$ with respect to d we find

$$d = \frac{k-1}{(k-1)\log \mu_k - \sum_{j=2}^{k-1} \log \mu_j} \tag{B.12}$$

In fact, this MLE estimator is biased; the unbiased estimator is Levina and Bickel (2005)

$$d = \mathbb{E}\left[\frac{k-2}{(k-1)\log \mu_k - \sum_{j=2}^{k-1} \log \mu_j}\right] \tag{B.13}$$

In practice, we can compute the RHS for all points in the manifold (after fixing some value for the number of neighbors k) and compute the mean. We display a histogram of the MLE estimates over many points in the data manifold for two examples in figure 17. The variance provides some measure of the errors. Alternatively, we could directly measure $\log P$ and evaluate the likelihood as a function of d. The variance of this estimator was studied in Levina and Bickel (2005). They also found numerically that it can be useful to tune of the value of k, as very small k overestimates ID while large k underestimates ID.

We can use these results to extend the TwoNN method in a simple way to general k. Marginalizing over all but μ_k, we find that

$$P(\mu_k) = \frac{(k-1)d}{\mu_k^{(k-1)d+1}} \left(\mu_k^d - 1\right)^{k-1} \tag{B.14}$$

which leads to the cumulative distribution

$$C(\mu_k) = \left(1 - \frac{1}{\mu_k^d}\right)^{k-1} \tag{B.15}$$

and the formula

$$d = \frac{\log\left(1 - C(\mu_k)^{\frac{1}{k-1}}\right)}{\log \mu_k} \tag{B.16}$$

for the kth nearest neighbor. This can be used as a cross-check for TwoNN. For examples of the relationship between the numerator and denominator with various k, and the relevant fits, see figure 16. Just as with MLE, we find empirically that larger k leads to smaller estimates of ID (see figure 21).

Appendix C. Examples and Tests of Intrinsic Dimension Estimation

The MLE and TwoNN methods have been tested and demonstrated by their authors Levina and Bickel (2005); Ansuini et al. (2019). We conduct a few tests with synthetic data. Then we provide some other examples of the ID measurement process, including errors, using our student/teacher, CIFAR10, and language data.

C.1 Tests on Synthetic Data

As a baseline test, we evaluate the TwoNN and MLE methods on synthetic datasets with dimensions ranging from 2 to 128, with results in figure 18. We display synthetic data on the hypercube $[0, 1]^d$ as well as a d-torus $S^1 \times S^1 \times \cdots \times S^1$ embedded in $2d$ dimensions (in the simplest way, by embedding each circle factor in 2 Euclidean dimensions).

We notice that 1) results are more accurate for smaller d, with quite reliable results for the TwoNN method for $d \lesssim 20$, 2) at large d all methods tend to underestimate the true ID, but 3) its certainly possible to both under and over-estimate the true ID, and measurements are not necessarily even monotonic with the number of points used for the measurement. We also see that for the torus the ID estimates are reasonably accurate even for dimensions ~ 100, though there's certainly no guarantee that this will hold for unknown data manifolds.

As other authors have noted Camastra and Staiano (2016), the ID is under-estimated on the hypercube, likely because cubes have sharp boundaries and corners which reduce the number of neighbors. Similarly, we believe that the ID is often over-estimated for the torus because (due to the curvature of the circles in the embedding space) points are often closer together than they would be in flat Euclidean space. We have also seen as shown in Levina and Bickel (2005) that for small k the MLE method typically overestimates ID. The NN method seems a bit less sensitive to k as compared to MLE.

C.2 Tests on Neural Network Activations

In all cases we measure ID from fully trained networks, and we always use students (not teachers) in that context. There are a large variety of potential statistical and systematic errors associated with these measurements:

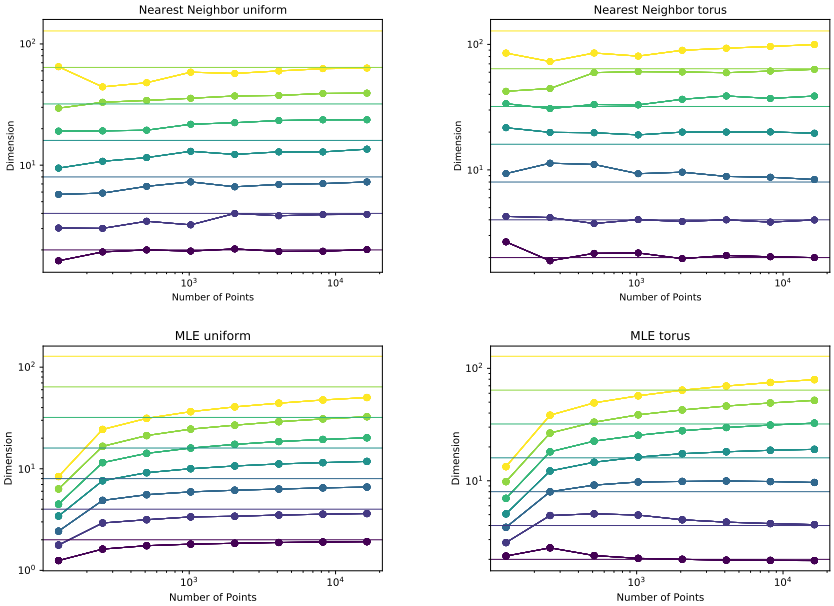

Figure 18: Here we show measured ID as a function of the number of points in the dataset used for the measurement, for both the TwoNN (top) and MLE (bottom) methods (with $k = 100$). The left plots show a uniform distribution in the hypercube $[0, 1]^d$, while the plot on the right show a d-torus embedded in $2d$ dimensions.

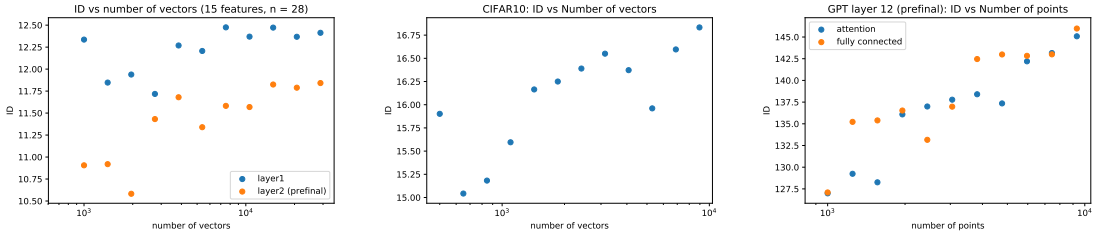

Figure 19: Variation of Intrinsic Dimension(ID) with number of vectors for a single student network (left), for the last layer of an $n = 5$ CNN trained on CIFAR10 (middle), and also for the last layer and last token of GPT (right). The student is of size $[15, 28, 28, 2]$ and was trained on teacher with 15 features.

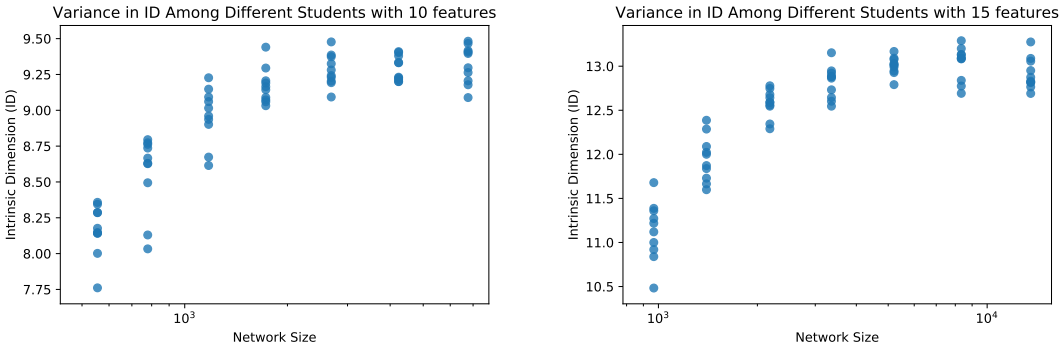

Figure 20: Variation of Intrinsic Dimension (ID) across network sizes for a single teacher. The figure on the left shows number of inputs features = 10 and the one on the right has 15. Each point on either figure is one student. All students on each figure are trained on the same teacher, but the teacher for the left and right figures are different.

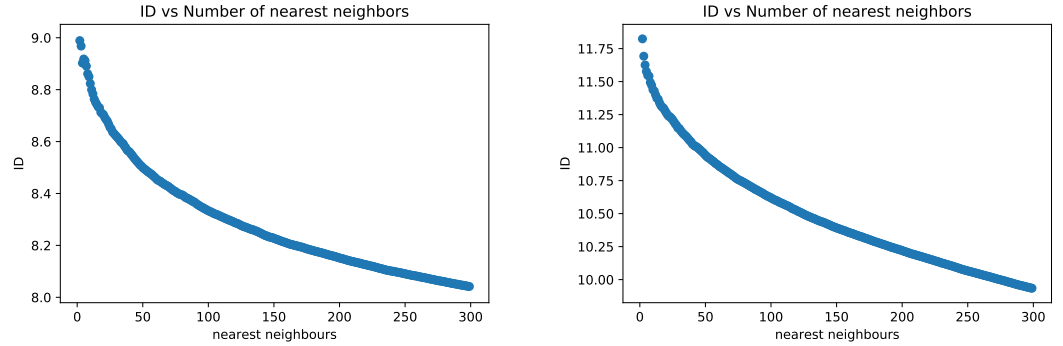

Figure 21: Variation of Intrinsic Dimension (ID) with number of neighbors used in the algorithm. The figure on the left shows a student of size $[20, 25, 25, 2]$ trained on a teacher with 10 features, while the one on the right has student shape $[15, 28, 28, 2]$ trained on teacher with 15 features.

- Variation among IDs measured from students of the same size and trained with the same teacher network (or dataset), but with different initialization (see figure 20).
- Variation of ID measurements among random groups of points sampled from the same data manifold
- Dependence of ID on the number of points used (and so the overall density) from the data manifold. More points samples shorter distance scales on the manifold. See figure 19.
- Dependence of ID on how many nearest neighbor points are used, either for NN (see figure 21) or MLE type estimation.
- Variation of ID from among points in different locations on the data data manifold (we show a histogram of results from MLE in figure 17)
- Dataset specific distinctions, eg from the same or different classes in an image classifier, or from the same or different text sequences in a language model (discussed in section 3.3)
- Dependence of ID measurements on the layer studied (see figures 9 and 19)

We provide some brief information about many of these sources of variation in the referenced plots. In most cases we find that the variation of the ID is small as long as it is measured with sufficiently many vectors. It would be interesting obtain a more precise theoretical and experimental characterization of these methods in the future.

But as evidenced by the synthetic examples in figure 18, this does not lead us to believe that the IDs are fully trustworthy, especially when they are measured to be large. Though the apparent statistical errors in ID measurements may seem small, there may be systematic errors that are more difficult to observe.

It's conceivable that deficiencies in ID measurement actually work to the advantage of the theory relating d and $4/\alpha$. For example, d tends to be underestimated when the data manifold has a boundary (or simply less support in some region), but this may also correlate with regions of the manifold where there really is less data, and these regions do not need to be modeled as precisely to achieve a good test loss. But we leave a more thorough investigation of such subtleties to future work.

References

Martín Abadi, Ashish Agarwal, Paul Barham, Eugene Brevdo, Zhifeng Chen, Craig Citro, Greg S. Corrado, Andy Davis, Jeffrey Dean, Matthieu Devin, Sanjay Ghemawat, Ian Goodfellow, Andrew Harp, Geoffrey Irving, Michael Isard, Yangqing Jia, Rafal Jozefowicz, Lukasz Kaiser, Manjunath Kudlur, Josh Levenberg, Dandelion Mané, Rajat Monga, Sherry Moore, Derek Murray, Chris Olah, Mike Schuster, Jonathon Shlens, Benoit Steiner, Ilya Sutskever, Kunal Talwar, Paul Tucker, Vincent Vanhoucke, Vijay Vasudevan, Fernanda Viégas, Oriol Vinyals, Pete Warden, Martin Wattenberg, Martin Wicke, Yuan Yu, and Xiaoqiang Zheng. TensorFlow: Large-scale machine learning on

heterogeneous systems, 2015. URL https://www.tensorflow.org/. Software available from tensorflow.org.

Alessio Ansuini, Alessandro Laio, Jakob H. Macke, and Davide Zoccolan. Intrinsic dimension of data representations in deep neural networks, 2019.

Ronen Basri and David Jacobs. Efficient representation of low-dimensional manifolds using deep networks, 2016.

GÃŠrard Biau. Analysis of a random forests model. *Journal of Machine Learning Research*, 13(Apr):1063–1095, 2012.

Peter J Bickel, Bo Li, et al. Local polynomial regression on unknown manifolds. In *Complex datasets and inverse problems*, pages 177–186. Institute of Mathematical Statistics, 2007.

Lars Buitinck, Gilles Louppe, Mathieu Blondel, Fabian Pedregosa, Andreas Mueller, Olivier Grisel, Vlad Niculae, Peter Prettenhofer, Alexandre Gramfort, Jaques Grobler, Robert Layton, Jake VanderPlas, Arnaud Joly, Brian Holt, and Gaël Varoquaux. API design for machine learning software: experiences from the scikit-learn project. In *ECML PKDD Workshop: Languages for Data Mining and Machine Learning*, pages 108–122, 2013.

Francesco Camastra and Antonino Staiano. Intrinsic dimension estimation: Advances and open problems. *Information Sciences*, 328:26–41, 2016.

Karl Cobbe, Christopher Hesse, Jacob Hilton, and John Schulman. Leveraging procedural generation to benchmark reinforcement learning, 2019.

Elena Facco, Maria d'Errico, Alex Rodriguez, and Alessandro Laio. Estimating the intrinsic dimension of datasets by a minimal neighborhood information. *Scientific Reports*, 7, 12 2017. doi: 10.1038/s41598-017-11873-y.

Joel Hestness, Sharan Narang, Newsha Ardalani, Gregory Diamos, Heewoo Jun, Hassan Kianinejad, Md. Mostofa Ali Patwary, Yang Yang, and Yanqi Zhou. Deep learning scaling is predictable, empirically, 2017.

Joel Hestness, Newsha Ardalani, and Gregory Diamos. Beyond human-level accuracy: computational challenges in deep learning. In *Proceedings of the 24th Symposium on Principles and Practice of Parallel Programming*, pages 1–14, 2019.

Andrew Ilyas, Shibani Santurkar, Dimitris Tsipras, Logan Engstrom, Brandon Tran, and Aleksander Madry. Adversarial examples are not bugs, they are features. In H. Wallach, H. Larochelle, A. Beygelzimer, F. d'Alché Buc, E. Fox, and R. Garnett, editors, *Advances in Neural Information Processing Systems 32*, pages 125–136. Curran Associates, Inc., 2019. URL http://papers.nips.cc/paper/8307-adversarial-examples-are-not-bugs-they-are-features.pdf.

Jared Kaplan, Sam McCandlish, Tom Henighan, Tom B. Brown, Benjamin Chess, Rewon Child, Scott Gray, Alec Radford, Jeffrey Wu, and Dario Amodei. Scaling laws for neural language models, 2020.

Diederik P. Kingma and Jimmy Ba. Adam: A method for stochastic optimization, 2014.

Alex Krizhevsky. Learning multiple layers of features from tiny images. Technical report, 2009.

Yann LeCun and Corinna Cortes. MNIST handwritten digit database. 2010. URL `http://yann.lecun.com/exdb/mnist/`.

Elizaveta Levina and Peter J Bickel. Maximum likelihood estimation of intrinsic dimension. In *Advances in neural information processing systems*, pages 777–784, 2005.

Chunyuan Li, Heerad Farkhoor, Rosanne Liu, and Jason Yosinski. Measuring the intrinsic dimension of objective landscapes, 2018.

Peter J. Liu, Mohammad Saleh, Etienne Pot, Ben Goodrich, Ryan Sepassi, Lukasz Kaiser, and Noam Shazeer. Generating wikipedia by summarizing long sequences. *arXiv:1801.10198 [cs]*, 2018. URL `http://arxiv.org/abs/1801.10198`.

Xingjun Ma, Yisen Wang, Michael E. Houle, Shuo Zhou, Sarah M. Erfani, Shu-Tao Xia, Sudanthi Wijewickrema, and James Bailey. Dimensionality-driven learning with noisy labels, 2018.

Guido F Montufar, Razvan Pascanu, Kyunghyun Cho, and Yoshua Bengio. On the number of linear regions of deep neural networks. In *Advances in neural information processing systems*, pages 2924–2932, 2014.

Yuval Netzer, Tao Wang, Adam Coates, Alessandro Bissacco, Bo Wu, and Andrew Y Ng. Reading digits in natural images with unsupervised feature learning. 2011.

Chris Olah, Nick Cammarata, Ludwig Schubert, Gabriel Goh, Michael Petrov, and Shan Carter. Zoom in: An introduction to circuits. *Distill*, 2020. doi: 10.23915/distill.00024.001. https://distill.pub/2020/circuits/zoom-in.

Alec Radford, Karthik Narasimhan, Tim Salimans, and Ilya Sutskever. Improving language understanding by generative pre-training. *URL https://s3-us-west-2. amazonaws. com/openai-assets/research-covers/languageunsupervised/language understanding paper. pdf*, 2018.

Alec Radford, Jeff Wu, Rewon Child, David Luan, Dario Amodei, and Ilya Sutskever. Language models are unsupervised multitask learners. *openai.com*, 2019.

Jonathan S. Rosenfeld, Amir Rosenfeld, Yonatan Belinkov, and Nir Shavit. A constructive prediction of the generalization error across scales, 2019.

Stefano Spigler, Mario Geiger, and Matthieu Wyart. Asymptotic learning curves of kernel methods: empirical data v.s. teacher-student paradigm, 2019.

Mingxing Tan and Quoc V. Le. Efficientnet: Rethinking model scaling for convolutional neural networks. *CoRR*, abs/1905.11946, 2019. URL `http://arxiv.org/abs/1905.11946`.

Ashish Vaswani, Noam Shazeer, Niki Parmar, Jakob Uszkoreit, Llion Jones, Aidan N Gomez, Ł ukasz Kaiser, and Illia Polosukhin. Attention is all you need. In I. Guyon, U. V. Luxburg, S. Bengio, H. Wallach, R. Fergus, S. Vishwanathan, and R. Garnett, editors, *Advances in Neural Information Processing Systems 30*, pages 5998–6008. Curran Associates, Inc., 2017. URL `http://papers.nips.cc/paper/7181-attention-is-all-you-need.pdf`.

Larry Wasserman. *All of nonparametric statistics*. Springer Science & Business Media, 2006.

Han Xiao, Kashif Rasul, and Roland Vollgraf. Fashion-mnist: a novel image dataset for benchmarking machine learning algorithms. 08 2017.